Gamow-Teller strength distributions in Xe isotopes

O. Moreno [1], R. Álvarez-Rodríguez [1], P. Sarriguren [1], E. Moya de Guerra [1,2], J. M. Udías [2] and J. R. Vignote [1,2]
[1] *Instituto de Estructura de la Materia. Consejo Superior de Investigaciones Científicas. Serrano 123, E-28006 Madrid, Spain*
[2] *Dpto. Física Atómica, Molecular y Nuclear. Facultad de Ciencias Físicas. Universidad Complutense de Madrid. Avda. Complutense s/n, E-28040 Madrid, Spain.*
(February 9, 2008)

The energy distributions of the Gamow-Teller strength are studied for even-even Xe isotopes with mass numbers from 124 to 142. A self-consistent microscopic formalism is used to generate the single particle basis, using a deformed Skyrme Hartree-Fock mean field with pairing correlations in BCS approximation. The Gamow-Teller (GT) transitions are obtained within a quasiparticle random phase approximation (QRPA) approach using a residual spin-isospin interaction in the particle-hole and particle-particle channels. We then discuss the pairing BCS treatment and the determination of the *ph* and *pp* residual interaction coupling constants. We study the GT^+ and GT^- strength distributions for the equilibrium nuclear shapes, which are an essential information for studies of charge-exchange reactions and double-β processes involving these isotopes.

PACS: 21.60.Jz, 23.40.-s, 27.60.+j

I. INTRODUCTION

The isotope ^{136}Xe has been recently used as a moving target colliding with a hydrogen gas jet in a first test to proof the feasibility of the EXL experimental approach at FAIR-GSI [1]. Charge-exchange (p,n) reactions on this Xe isotope were consequently measured. Although this kind of facilities are intended to explore highly unstable nuclei, some stable isotopes like those under study here are normally used as initial test targets. Therefore, having reliable information on their nuclear structure turns out to be of primary importance. From ^{136}Xe, we extend our study to other stable isotopes, $^{124-134}$Xe, and also to the neutron-rich region ^{138,140,142}Xe. The latter undergo β^--decay and their half-lives provide us with another piece of experimental information.

Gamow-Teller transition matrix elements can be extracted from the measured forward-angle charge-exchange data [2]. At high incident energies and at forward angles, the nuclear states are probed at small momentum transfer. Therefore, only the central parts of the isovector effective interaction contribute to the cross-section. Furthermore, because of the small momentum transfer, a multipole expansion leads to a simple relation between the measured 0^o cross sections and the corresponding allowed β-decay transition rates (L=0). Assuming that even taking into account the projectile distortion effects in DWBA the transition amplitudes would still approximately factorize into a nuclear reaction part and a nuclear structure part, the 0^o charge-exchange cross sections are proportional to the corresponding Fermi and Gamow-Teller matrix elements. The proportionality factor is parametrized in terms of a distortion factor, a kinematic factor and a volume integral of the effective interaction [2].

Theoretical $GT^{\pm}$ strength distributions, as the ones discussed here, can therefore be used to predict cross sections of various charge-exchange reactions under the appropriate kinematic conditions. Some of the charge-exchange reactions corresponding to GT^- processes are:
^{136}Xe(p,n)^{136}Cs ; ^{136}Xe(^{3}He,^{3}H)^{136}Cs ; ^{136}Xe(d,2n)^{136}Cs ;
while some examples of those corresponding to GT^+ transitions are:
^{136}Xe(n,p)^{136}I ; ^{136}Xe(^{3}H,^{3}He)^{136}I ; ^{136}Xe(d,2p)^{136}I.

In addition, the Xe isotopes are of special interest regarding double β processes [3]. Different nuclear models have been developed by many groups to calculate quantitatively the double β matrix elements, as described in recent review articles [4]. Table I shows all the transitions of this type involving Xe isotopes as parents or daughters. The $GT^{\pm}$ strength distributions which will be obtained here can be used to calculate the transition amplitudes of the initial and final ground states going to the virtual QRPA-excited states of the intermediate odd-odd nucleus. After computing the overlap between the intermediate states coming from the parent and from the daughter nuclei, the two-neutrino double beta decay matrix elements as well as the half-lives can be calculated. Such a calculation has indeed been carried out in [8] for ^{128}Xe, ^{130}Xe and ^{136}Xe, which are β^-/β^- parents or daughters.

Finally, Xe isotopes are of considerable interest because they belong to a typical shape transitional region [9], in which there are experimental indications of triaxial deformation in some isotopes [10]. Present theoretical triaxial calculations are mainly based on algebraic models [11]. Nevertheless, in this work we assume axial symmetry. As we shall see, for the deformed Xe isotopes with two equilibrium shapes there are no critical changes in the Gamow-Teller strengths at these two shapes, and a similar behavior may be expected when considering possible triaxial shapes. In any case, axial deformation is a crucial ingredient of the formalism that gives rise to new features in the Gamow-Teller strength distributions different from those obtained within a spherical treatment.

Although some of the isotopes studied may be spherical, in this work we are not restricted to those but we deal with a large number of Xe isotopes whose equilibrium shapes are unknown. For most of the isotopes considered here, there is no clear experimental evidence of whether they are spherical or deformed. Under these circumstances, a deformed approach is always preferable over a spherical one because a deformed formalism contains the spherical shape as a particular solution.

We have also found in the past [12,13] that the GT strength distributions may depend, in some cases significantly, on the deformation of the decaying nucleus. But we notice that this dependence has to be studied case by case since it is very sensitive to the fragmentation and crossing of levels generated by the deformation. We think it is indeed worth studying the degree of sensitivity of the GT strength of these Xe isotopes to deformation.

Following this introduction we present in Sec. II a brief description of the theoretical framework. Sec. III includes our results regarding HF+BCS energies and GT$^{\pm}$ strength distributions, together with a discussion on the pairing treatment. Finally, Sec. IV contains the main conclusions of our work.

II. THEORETICAL FRAMEWORK

We describe here briefly the theoretical formalism used, whose details can be found in ref. [12]. We carry out a deformed Hartree-Fock calculation with the effective nucleon-nucleon density-dependent Skyrme interaction Sk3 [14], assuming axial deformation and time reversal symmetry. The single-particle wave functions are expanded in terms of the eigenstates of an axially symmetric harmonic oscillator in cylindrical coordinates using eleven major shells. Pairing correlations between like nucleons are included in BCS approximation either taking fixed pairing gap parameters (Δ_π for protons and Δ_ν for neutrons) or taking fixed pairing strength parameters (G_π and G_ν respectively). We refer to these two types of calculations as HF(Sk3)+BCS(Δ) and HF(Sk3)+BCS(G), respectively. They yield single particle energies and wave functions together with their occupation probabilities for protons and neutrons separately. A quadrupole constrained HF+BCS calculation [15], where the intrinsic quadrupole moment is constrained, is also performed to obtain the deformation dependence of the ground state energy.

The pairing energy gaps Δ are determined phenomenologically, and the pairing strengths G are obtained from them in an indirect way, as will be described later on. Within BCS approximation, both parameters are related by the so called gap equation:

$$\Delta = G \sum_i u_i v_i \,, \tag{2.1}$$

where v_i y u_i are occupation and non-occupation probability amplitudes of the i^{th} single particle level subject to the condition $v_i^2 + u_i^2 = 1$. In order to determine the value of G that reproduces a given value of Δ, one should take into account that this depends on the active energy range and number of levels considered. In our case, we include all HF single particle sates in our basis above and below Fermi level. It is important to stress that the occupation probability amplitudes are computed in each iteration of the HF method, and are used to calculate the one-body density and mean field of the next iteration, so that one gets new single-particle wave functions, energies and occupation numbers at each iteration. Therefore, the selfconsistent determination of the binding energy and deformation includes pairing correlations from the beginning.

To describe Gamow-Teller excitations we add to the quasiparticle mean field a separable spin-isospin residual interaction in the particle-hole (ph) and particle-particle (pp) channels, which is treated within QRPA. The advantage of using separable forces is that the QRPA energy eigenvalue problem is reduced to find the roots of an algebraic equation. The ph part

$$V_{GT}^{ph} = 2\chi_{GT}^{ph} \sum_{K=0,\pm1} (-1)^K \beta_K^+ \beta_{-K}^-, \qquad \beta_K^+ = \sum_{\pi\nu} \langle \nu \,|\sigma_K|\, \pi \rangle \, a_\nu^+ a_\pi \,, \tag{2.2}$$

is responsible for the position and structure of the GT resonance [12,16–18]. The corresponding coupling constant, χ_{ph}^{GT} is obtained in a consistent way from the same energy density functional as the Hartree-Fock mean field through a

second derivative with respect to the nucleonic density and averaging the contact interaction over the nuclear volume [12]. The *pp* part consists of a proton-neutron pairing force, which we introduce as a separable force [17,19,20],

$$V_{GT}^{pp} = -2\kappa_{GT}^{pp} \sum_{K} (-1)^K P_K^+ P_{-K}, \qquad P_K^+ = \sum_{\pi\nu} \left\langle \pi \left| (\sigma_K)^+ \right| \nu \right\rangle a_\nu^+ a_{\bar{\pi}}^+ \,. \tag{2.3}$$

The coupling constant κ_{pp}^{GT} may in principle be derived consistently with the HFB or HF+BCS mean field through a second derivative with respect to the pairing tensor of the energy density functional. This derivation would be analogous to the way in which the *ph* force is obtained as the second derivative with respect to the density. In our theoretical scheme the proton-neutron pairing interaction is neglected in the construction of the mean field to avoid mixing of even-even and odd-odd isotopes in the intrinsic state. Only pairing between like particles is included in the BCS approximation. This implies that the particle-particle interaction in the proton-neutron channel is in principle undetermined. Therefore the coupling constant κ_{pp}^{GT} is fitted to the phenomenology, as for example to reproduce half-lives as it is usually done [17,18].

The pnQRPA phonon operator for GT excitations in even-even nuclei is written as

$$\Gamma_{\omega_K}^+ = \sum_{\pi\nu} \left[X_{\pi\nu}^{\omega_K} \alpha_\nu^+ \alpha_{\bar{\pi}}^+ - Y_{\pi\nu}^{\omega_K} \alpha_{\bar{\nu}} \alpha_\pi \right] \,, \tag{2.4}$$

where π and ν stand for proton and neutron, respectively, α^+ (α) are quasiparticle creation (annihilation) operators, ω_K are the RPA excitation energies, and $X_{\pi\nu}^{\omega_K}, Y_{\pi\nu}^{\omega_K}$ the forward and backward amplitudes, respectively. It satisfies

$$\Gamma_{\omega_K} |0\rangle = 0 \,; \qquad \Gamma_{\omega_K}^+ |0\rangle = |\omega_K\rangle \,. \tag{2.5}$$

when acting on the QRPA ground state of the parent nucleus $|0\rangle$.

The technical details to solve the QRPA equations are well described in Refs. [12,16,19]. Here we only mention that, because of the use of separable residual forces, the solutions of the QRPA equations are found by solving first a dispersion relation, which is an algebraic equation of fourth order in the excitation energy ω. Then, for each value of the energy, the GT transition amplitudes in the intrinsic frame connecting the ground state $|0\rangle$ to one phonon states in the daughter nucleus $|\omega_K\rangle$, are determined by using the normalization conditions of the phonon amplitudes. They are given by

$$\left\langle \omega_K | \beta_K^\pm | 0 \right\rangle = \mp M_\pm^{\omega_K} \,, \tag{2.6}$$

where

$$M_-^{\omega_K} = \sum_{\pi\nu} \left(q_{\pi\nu} X_{\pi\nu}^{\omega_K} + \tilde{q}_{\pi\nu} Y_{\pi\nu}^{\omega_K} \right) \,; \qquad M_+^{\omega_K} = \sum_{\pi\nu} \left(\tilde{q}_{\pi\nu} X_{\pi\nu}^{\omega_K} + q_{\pi\nu} Y_{\pi\nu}^{\omega_K} \right) \,, \tag{2.7}$$

with

$$\tilde{q}_{\pi\nu} = u_\nu v_\pi \Sigma_K^{\nu\pi}; \quad q_{\pi\nu} = v_\nu u_\pi \Sigma_K^{\nu\pi} \,; \qquad \Sigma_K^{\nu\pi} = \left\langle \nu \left| \sigma_K \right| \pi \right\rangle \,, \tag{2.8}$$

It is a simple matter to find out that the Ikeda sum rule

$$\sum_{\omega_K} \left[\left(M_-^{\omega_K} \right)^2 - \left(M_+^{\omega_K} \right)^2 \right] = 3(N-Z) \tag{2.9}$$

holds in RPA approximation provided all the eigenvalues contained in the basis space are included in the sum, so that the orthonormalization conditions are satisfied. In practice, the strength functions are calculated up to an energy $\omega < E_{\rm cut}$, where $E_{\rm cut}$ is such that Ikeda sum rule is fulfilled up to a few per thousand discrepancy. Typical energies used in our calculations are $E_{\rm cut} = 30$ MeV. The number of configurations involved in this mass region for this energy range is typically over one thousand.

Once the intrinsic amplitudes in Eq. (2.6) are calculated, the Gamow-Teller strength $B(GT)$ in the laboratory frame for a transition $I_i K_i (0^+ 0) \rightarrow I_f K_f (1^+ K)$ can be obtained as

$$B^\pm(GT) = \sum_{M_i, M_f, \mu} \left| \left\langle I_f M_f \left| \beta_\mu^\pm \right| I_i M_i \right\rangle \right|^2 = \left\{ \delta_{K_f,0} \left\langle \phi_{K_f} \left| \beta_0^\pm \right| \phi_0 \right\rangle^2 + 2\delta_{K_f,1} \left\langle \phi_{K_f} \left| \beta_1^\pm \right| \phi_0 \right\rangle^2 \right\} \,. \tag{2.10}$$

To obtain this expression we have used the initial and final states in the laboratory frame expressed in terms of the intrinsic states $|\phi_K>$, using the Bohr and Mottelson factorization [21]. Theoretical β^--decay half-lives are calculated

by summing up all the energetically allowed transition probabilities in (2.10), in units of $g_A^2/4\pi$, weighted with phase space factors, up to states in the daughter nucleus with excitation energies below the Q_{β^-} window.

One may wonder whether, in deformed nuclei, the calculated GT strengths may contain spurious contributions from higher angular momentum components in the initial and final wave functions. As mentioned above, the GT strengths are calculated in the laboratory frame in the factorization approximation of Bohr and Mottelson. Using angular momentum projection techniques [22], the angular momentum projection can be carried out through an expansion in inverse powers of the angular momentum operator component perpendicular to the symmetry axis $< J_\perp^2 >$. This expansion, to lower order, provides a factorization approximation formally identical to that of Bohr and Mottelson. Thus, the effect of angular momentum projection is to a large extent taken into account. An upper bound to contributions from higher angular momentum components is proportional to $< J_\perp^2 >^{-2}$, with values of $< J_\perp^2 >$ ranging from 10 to 40 in the case of the deformed Xe isotopes. Therefore, exact angular momentum projection in deformed Xe isotopes would lead in all cases to less than a few percent effect in the GT strengths. In the cases where the shape is spherical, there are not high angular momentum contributions to the GT strengths.

It may be questioned whether it is correct to introduce additional BCS parameters and residual interactions on top of the Skyrme interaction, which is already an effective interaction. Indeed, if the effective force used in constructing the mean field were to be the most general possible interaction, one should not include additional parameters. However, this is not the case for the Skyrme interaction. The parameters of the Skyrme force are determined by requiring that they reproduce the nuclear compressibility, as well as the total binding energies and charge radii of magic nuclei in spherical selfconsistent calculations. It is well known that the effective Skyrme interaction and its existent parametrizations are suitable to generate the optimal HF mean field of spherical and deformed nuclei [14,23]. The particle and hole eigenstates of the mean field, which form the canonical basis, have highly nontrivial wave functions that contain a mixture of many harmonic oscillator shells, when expanded into a harmonic oscillator basis. In addition to deformation, for non-closed shell nuclei, one has to take into account the pairing correlation effects which are important when the level density around the Fermi level becomes large.

It is also well known that the effective Skyrme interaction is not suitable to generate the quasiparticle mean field, since in the fit of the Skyrme forces no attention is paid to the realistic character of the pairing matrix elements, and extensions of the Skyrme HF method have been developed over the years. To include pairing correlations in the mean field one possibility is to do Hartree-Fock-Bogoliubov calculations using either finite range forces, like the Gogny force, or contact density dependent pairing interactions [24]. All of them are extensions of the Skyrme forces specifically designed for this purpose. The other possibility is to perform BCS calculations in the canonical basis using either phenomenological fixed gap parameters or fixed pairing strengths, as originally proposed by Vautherin. This is the path followed in our paper. This path has been proved to be successful to study the properties of ground state and low spin excited states in open shell nuclei [12,14,23,25].

Concerning the residual interactions, we mentioned above that the same effective Skyrme interaction is used to generate a separable particle-hole residual interaction. The separable interaction simplifies enormously the calculation and still contains the main characteristics of the contact force. The quasiparticle energy density functional obtained with the effective Skyrme and pairing interactions that we used does not contain any dependence on particle-particle interactions in the proton-neutron channel. Therefore we have to introduce a proton-neutron particle-particle residual interaction in the usual way as a separable force with a coupling strength that we fit to the measured half lives. We would like to recall that a bridge between Skyrme HF and RPA calculations for excited states was established long time ago [26] by using a particle-hole force in the RPA, which is determined by the second derivatives of the HF energy with respect to the density. But there is no guarantee that the derived force is good for excited states. This is so because Skyrme forces are constructed for the description of ground state properties. Finally, we would like to notice that similar schemes based on Skyrme HF+BCS+RPA have been frequently used in the literature with successful results [27].

III. RESULTS AND DISCUSSION

A. Equilibrium deformations

A deformed Hartree-Fock mean field calculation is performed using a Sk3 Skyrme force with a constraint of the quadrupole deformation given by the parameter $\beta = \sqrt{\pi/5}\, Q_p/(Z\langle r^2\rangle)$, where Q_p is the proton quadrupole moment and $\langle r^2\rangle$ is the charge mean square radius. A pairing interaction between like nucleons within BCS approximation is also included, keeping fixed the pairing energy gap (Δ) or the pairing strength (G). From this calculation we obtain the ground state energy as a function of the quadrupole deformation β.

In principle, when a pairing force with fixed strength $G_{\pi,\nu}$ is used, the pairing energy gaps $\Delta_{\pi,\nu}$ depend on the strength of the pairing interaction as well as on the occupation amplitudes of the single-particle states (see Eq.(2.1)). This last condition amounts to say that pairing energy gaps are deformation-dependent. Actually, we obtain these gaps first phenomenologically from the odd-even mass differences by means of a symmetric five term formula involving experimental binding energies [7], and keep them fixed to carry out a deformation-constrained HF+BCS(Δ) calculation. Next we fix the pairing strength so as to reproduce the gap parameters at the deformation of the ground state, and we carry out a deformation-constrained HF+BCS(G) calculation. In this way we perform a fixed pairing strength calculation, which is conceptually more appealing, but still profiting from the experimental information available for the gaps.

Fig. 1 shows the HF+BCS energies for $^{124-142}$Xe, using Sk3 Skyrme interaction. The pairing interaction is included in both fixed gap (dashed line) and fixed strength (solid line) treatments, each of them in a different curve whose absolute minima have been separated 1 MeV for a better comparison. For the same isotope, both curves show energy minima at very similar deformations, the ones corresponding to the fixed pairing strength treatment being slightly smaller in absolute value. One can also observe that the energy barrier at the spherical region of $^{124-132}$Xe and of $^{140-142}$Xe is less pronounced when the pairing strength is fixed, and in this case both minima have a very similar energy (the prolate one being generally the ground state, except for ^{126}Xe). As the mass number increases from A=124 to A=138, the deformations of the equilibrium shapes decrease and eventually converge to a spherical shape. The two final isotopes show only one equilibrium deformation in the prolate region.

Underneath each of these energy-deformation graphs we plot the corresponding pairing gaps as a function of the quadrupole deformation for the fixed pairing strength calculation. The vertical lines join the ground states from fixed gap treatment with the corresponding pairing gaps at this deformation from the fixed strength treatment. These values are those coming from the aforementioned odd-even experimental mass differences.

In our calculations with fixed G values the binding energies show a tendency to increase at those deformations where the pairing gaps reach a minimum. This looks contradictory since one may expect the opposite because the smaller the pairing gap is, the lower is the contribution of the pairing energy to the total binding energy. However, it indicates that the minima of the pairing gaps appear at similar deformation to that where the volume and the spin-orbit term contributions to the binding energy are maximum. On the other hand, comparing calculations with G fixed to those with Δ fixed, one sees in 1 that for β values where Δ takes larger values the binding energy increases more compared to that obtained with lower (Δ fixed) value.

In Table II we show the quadrupole deformation β of the equilibrium shapes according to the HF(Sk3)+BCS(Δ) and HF(Sk3)+BCS(G) calculations. We also show for comparison the results from independent theoretical calculations obtained from selfconsistent relativistic calculations [29] as well as from phenomenological nonrelativistic calculations [30]. These results also indicate the existence of deformed solutions, which agree with those obtained here. Upper limits of the ground state deformation obtained from experimental B(E, $2_1^+ \rightarrow 0_1^+$) transitions are also included [28]. Table III shows the pairing gaps, obtained from experimental binding energies, and the pairing strengths reproducing these gaps at the ground state deformation.

B. Gamow-Teller strength distributions

The spin-isospin residual interactions in the particle-hole and particle-particle channels are treated here within a quasiparticle random phase approximation. The particle-hole residual interaction coupling constant χ_{ph} is obtained consistently with the Hartree-Fock mean field, and their values vary from 0.21 MeV in ^{124}Xe to 0.19 MeV in ^{142}Xe. We have used an average value for all the isotopes under study, $\chi_{ph} = 0.2$ MeV. In the case of the particle-particle residual interaction, we have chosen the value of the coupling constant κ_{pp} so as to reproduce the experimental half-lives of the three unstable Xe isotopes: ^{138}Xe ($T_{1/2}$=844.8 s), ^{140}Xe ($T_{1/2}$=13.60 s) and ^{142}Xe ($T_{1/2}$=1.22 s). A good agreement between calculated and experimental β^- half-lives for the three isotopes is reached with κ_{pp}=0.07 MeV, provided we use the standard attenuation factor 0.77 for spin matrix elements as in previous works.

The single particle energies and occupation probabilities at the equilibrium nuclear shapes are obtained from a HF(Sk3)+BCS(G) calculation. Fig. 2 shows GT^- strengths (in $g_A^2/(4\pi)$ units) as a function of the excitation energy of the daughter nucleus after the transition. Discrete and gaussian-folded distributions are shown, the latter being more suited to compare with experimental results regarding the GT strengths themselves or the cross sections of charge-exchange reactions obtained from them. The range of the excitation energy from 0 to 30 MeV includes the resonance, which appears at around 13 MeV in ^{124}Xe and moves slightly toward higher excitation energies as the mass number increases, reaching 25 MeV in ^{142}Xe.

Fig. 3 shows the same calculations but for GT^+ transitions. As expected from the Ikeda sum rule, Eq. (2.9), the scale of the strengths is much smaller in this case. Table IV contains the summed $GT^\pm$ strengths, their difference,

the value of $3(N-Z)$ and the fulfillment of the Ikeda sum rule in percentage for the prolate shape of every isotope (which is generally the ground state), and for the oblate shape when there is a second minimum. The Ikeda sum rule is fulfilled up to a very high degree of accuracy in all the cases.

The fragmentation observed in the GT^+ strength is reduced as the prolate energy minimum moves to the spherical region (^{134,136,138}Xe). A double peak structure becomes then apparent, which was responsible for the larger width of these resonances in comparison with the ones in GT^- distributions. A second peak with less strength, in the near spherical shapes, appears 8 MeV below the biggest one and moves accordingly with it as the mass number changes. It is worth noticing the large single peak which appears at very low excitation energies in ^{126}Xe and also in ^{124}Xe, reaching in the prolate shape of this last case a strength of 0.34 $g_A^2/(4\pi)$, as indicated in the figure. This strength corresponds to a dominant GT transition from a $K^\pi = 9/2^+$ proton state to a $K^\pi = 7/2^+$ neutron state connecting the proton $g_{9/2}$ shell with the neutron $g_{7/2}$ shell. The occupation probability of the neutron state is small enough to allow the transition in ^{124}Xe and ^{126}Xe, but when the number of neutrons increases, this state becomes blocked for GT transitions.

From the $GT^\pm$ profiles of $^{124-132}$Xe it is obvious that no clear distinction can be made between oblate and prolate deformations. It is only possible to distinguish both deformations in some cases when small energy windows are explored, as for example in the low $B(GT^+)$ energy window of ^{124,126}Xe. Similar studies on the effect of deformation in the GT strength distributions were done in the neutron-deficient Hg-Pb-Po region [31], and in the A$\simeq$70 mass region [12].

The effect of deformation on the GT strength distributions can be observed more clearly in Fig. 4, where we compare spherical and deformed QRPA results. We show the examples of ^{128}Xe, where two equilibrium shapes, oblate and prolate, are obtained, and ^{140}Xe, where a prolate shape is predicted. In Fig. 4 plots upward correspond to deformed calculations with prolate shapes, while plots downward correspond to spherical calculations. The left panels show the GT^- strengths and the right ones the GT^+ strengths. As we can see in Fig. 4 the main effect of deformation is the stronger fragmentation of the strength, which is particularly clear on the GT^+ strength distributions because of the smaller scale. The positions of the peaks are also changed from spherical to deformed in a different way for each case.

In order to compare the GT strength distributions obtained here with those coming from a HF(Sk3)+BCS(Δ) calculation of the single particle levels, we show in Fig. 5 the distributions corresponding to both BCS pairing treatments (fixed gap and fixed strength) for the prolate and oblate equilibrium shapes of ^{128}Xe. The results are very similar, as could be expected given the fact that the equilibrium nuclear shapes occur at very similar deformations and binding energies in both BCS treatments (see Fig. 1). In particular, for the prolate shape both distributions are almost identical as expected because the values of the $G_{\pi,\nu}$ parameters were chosen to reproduce the $\Delta_{\pi,\nu}$ parameters precisely at this deformation. It is interesting to know that also at the oblate minimum these pairing strengths nearly reproduce the values of the phenomenological pairing gaps, since as seen in Fig. 1 they are very close to the ones at the prolate minimum. Therefore the distributions for the oblate case with both pairing treatments are also very similar. In the case of spherical equilibrium shapes, as for example ^{136}Xe, the GT strength distributions from fixed pairing gap and fixed pairing strength calculations are indistinguishable.

IV. SUMMARY AND CONCLUSIONS

The Xe isotopes are of considerable theoretical interest because they participate in a variety of double-beta decay processes and because they belong to a nuclear shape transitional region. In addition, from the experimental point of view, the stable Xe isotopes have been used as moving targets in charge-exchange reactions to test new facilities, where the unstable Xe isotopes will be explored in the near future. The present work has addressed these topics by predicting stable nuclear shapes and GT strength distributions, which are a fundamental tool to calculate single and double beta transition matrix elements and half-lives, as well as cross sections of charge-exchange reactions under the appropriate kinematic conditions.

For even-even Xe isotopes with mass numbers from 124 to 142, we have studied the GT strength distributions using a deformed pnQRPA formalism with *ph* and *pp* spin-isospin separable residual interactions. The quasiparticle mean field is obtained from an axially deformed HF approach, with the Skyrme interaction Sk3, including pairing correlations between like-nucleons in BCS approximation using either fixed gaps ($\Delta_{\pi,\nu}$) or fixed pairing interaction strength ($G_{\pi,\nu}$). The HF+BCS mean field has been also used to consistently determine the *ph* coupling constant for every isotope, whose average value has been finally used for all of them. The *pp* coupling constant has been fixed to approximately reproduce the half-life of the three β^--unstable Xe isotopes included in this work.

From the energy-deformation curves, an oblate-prolate shape coexistence is predicted in $^{124-132}$Xe with a low energy barrier between them. $^{134-138}$Xe are predicted to be spherical, whereas the prolate shape seems to be strongly favored in $^{140-142}$Xe. In general, a fixed pairing strength calculation increases the binding energy of the spherical shape

region. The deformation dependence of the pairing energy gaps from a fixed pairing strength calculation has been also shown. The self-consistent quadrupole deformations of the ground state derived within the HF+BCS procedure are in agreement with independent theoretical calculations as well as with the experimental upper bounds extracted from B(E2) transitions in the whole chain of Xe isotopes under study.

The GT^- strength distributions for the equilibrium shapes are dominated by a single peak moving to higher excitation energies and gathering more strength as the number of neutrons increases, as expected. In the cases where two equilibrium shapes are predicted, there is no strong dependence of the GT strength distribution on the equilibrium shape, at least when a wide range of excitation energy is considered.

In the case of the GT^+ transitions, the strength is more fragmented, giving rise to a richer structure in the energy distribution. This fragmentation decreases as the energy minima move to the spherical region, where a double-peaked resonance appears as observed in $^{134-138}$Xe. The lightest isotopes, ^{124}Xe and ^{126}Xe, show a very high peak from a single transition at very low excitation energies, but this transition is blocked in the isotopes with higher number of neutrons. With such a complex structure, the influence of the sign of the nuclear deformation (oblate or prolate) in $^{124-132}$Xe is more apparent on the GT^+ strength distributions than on the GT^- transitions, but in any case it does not seem to be critical. However, the GT strength distributions obtained from spherical or deformed shapes show different features related to the energy location of the main peaks and to the fragmentation of the strength. From the accumulated $GT^\pm$ strengths up to 30 MeV of excitation energy, it has been shown that the Ikeda sum rule is fulfilled up to a very high percentage (see table IV).

Theoretical studies of GT strengths and related observables as, in particular, charge-exchange reaction cross sections are necessary to help in the event simulation work of these kind of processes, that will be measured at the new FAIR-GSI facility. Theoretical work on this direction is in progress.

Acknowledgments

This work was supported by Ministerio de Educación y Ciencia (Spain) under contracts FIS2005-00640 and BFM2003-04147-C02-01. O.M. thanks Ministerio de Educación y Ciencia (Spain) for financial support. R.A.R. thanks I3P Programme (CSIC, Spain) for financial support. We also acknowledge participation in the European Collaborations EURONS (RII3-506065), ILIAS (RII3-CT-2004-506222), and INTAS-03-54-6545.

[1] EXL Technical Report, private communication.
[2] C.D. Goodman, C.A. Goulding, M.B. Greenfield, J. Rapaport, D.E. Bainum, C.C. Foster, W.G. Love, F. Petrovich, Phys. Rev. Lett. **44**, 1755 (1980); T.N. Taddeucci, C.A. Goulding, T.A. Carey, R.C. Byrd, C.D Goodman, C. Gaarde, J. Larsen, D. Horen, J. Rapaport and E. Sugarbaker, Nucl. Phys. A **469**, 125 (1987); F. Osterfeld, Rev. Mod. Phys. **64**, 491 (1992).
[3] H. Ejiri, Phys. Rep. **338**, 265 (2000).
[4] A. Faessler, F. Simkovic, J. Phys. G **24**, 2139 (1998); J. Suhonen, O. Civitarese, Phys. Rep. **300**, 123 (1998); S.R. Elliott and P. Vogel, Annu. Rev. Nucl. Part. Sci. **52**, 115 (2002); J.D. Vergados, Phys. Rep. **361**, 1 (2002); H.V. Klapdor-Kleingrothaus, *Sixty Years of Double Beta Decay*, (World Scientific, Singapore, 2001).
[5] V.I. Tretyak and Y.G. Zdesenko, At. Data and Nucl. Data Tables **80**, 83 (2002).
[6] A.S. Barabash, nucl-ex/0602009.
[7] G. Audi, O. Bersillon, J. Blachot and A.H. Wapstra, Nucl. Phys. A **729**, 3 (2003).
[8] R. Alvarez-Rodriguez, P. Sarriguren, E. Moya de Guerra, L. Pacearescu, Amand Faessler, F. Šimkovic, Phys. Rev. C, **70**, 064309 (2004).
[9] R. Wyss *et al.*, Nucl. Phys. A **505**, 337 (1989); N. Yoshinaga, K. Higashiyama, Phys. Rev. C **69**, 054309 (2004).
[10] W. Lieberz, A. Dewald, W. Frank, A. Gelberg, W. Krips, D. Lieberz, R. Wirowski, P. von Brentano, Phys. Lett. B **240**, 38 (1990).
[11] X.W. Pan, J.L. Ping, D.H. Feng, J.Q. Chen, C.L Wu and M.W. Guidry, Phys. Rev. C **53**, 715 (1996).
[12] P. Sarriguren, E. Moya de Guerra, A. Escuderos and A.C. Carrizo, Nucl. Phys. A **635**, 55 (1998); P. Sarriguren, E. Moya de Guerra and A. Escuderos, Nucl. Phys. A **658**, 13 (1999); Nucl. Phys. A **691**, 631 (2001); Phys. Rev. C **64**, 064306 (2001).
[13] E. Poirier *et al.*, Phys. Rev. C **69**, 034307 (2004); E. Nacher *et al.*, Phys. Rev. Lett. **92**, 232501 (2004).
[14] M. Beiner, H. Flocard, N. Van Giai and P. Quentin, Nucl. Phys. A **238**, 29 (1975).
[15] H. Flocard, P. Quentin, A.K. Kerman and D. Vautherin, Nucl. Phys. A **203**, 433 (1973).
[16] J. Krumlinde and P. Moeller, Nucl. Phys. A **417**, 419 (1984); P. Moeller and J. Randrup, Nucl. Phys. A **514**, 1 (1990).
[17] M. Hirsch, A. Staudt, K. Muto and H.V. Klapdor-Kleingrothaus, Nucl. Phys. **A535**, 62 (1991).
[18] H. Homma, E. Bender, M. Hirsch, K. Muto, H.V. Klapdor-Kleingrothaus and T. Oda, Phys. Rev. C **54**, 2972 (1996).
[19] K. Muto, E. Bender, T. Oda and H.V. Klapdor-Kleingrothaus, Z. Phys. A **341**, 407 (1992).
[20] J. Engel, P. Vogel and M.R. Zirnbauer, Phys. Rev. C **37**, 731 (1988); V.A. Kuz'min and V.G. Soloviev, Nucl. Phys. A **486**, 118 (1988).
[21] A. Bohr and B. Mottelson, *Nuclear Structure*, (Benjamin, New York 1975).
[22] E. Moya de Guerra, Phys. Rep. **138**, 293 (1986).
[23] D. Vautherin and D.M. Brink, Phys. Rev. C **5**, 626 (1972); D. Vautherin, Phys. Rev. C **7**, 296 (1973); J. Negele and D. Vautherin, Phys. Rev. C **5**, 1472 (1972); C **11**, 1031 (1975); P. Quentin, H. Flocard, Ann. Rev. Nucl. Part. Sci. **28**, 523 (1978); J. Friedrich and P.-. Reinhard, Phys. Rev. C **33**, 335 (1986); E. Chabanat, P. Bonche, P. Haensel, J. Meyer and R. Schaeffer, Phys. Rev. C **627**, 710 (1997); Nucl. Phys. A **635**, 231 (1998).
[24] G.F. Bertsch and H. Esbensen, Ann. Phys. (N.Y.) **209**, 327 (1991); E. Garrido, P. Sarriguren, E. Moya de Guerra and P. Schuck, Phys. Rev. C **60**, 064312 (1999).
[25] P. Sarriguren, E. Moya de Guerra and R. Nojarov, Phys. Rev. C **54**, 690 (1996).
[26] G.F. Bertsch and S.F. Tsai, Phys. Rep. **18**, 127 (1975); S. Krewald, V. Klemt, J. Speth and A. Faessler, Nucl. Phys. A **281**, 166 (1977).
[27] I. Hamamoto and H. Sagawa, Phys. Rev. C **60**, 064314 (1999); M. Bender, J. Dobaczewski, J. Engel and W. Nazarewicz, Phys. Rev. C **65**, 054322 (2002); N.Van Giai, Ch. Stoyanov and V.V. Voronov, Phys. Rev. C **57**, 1204 (1998).
[28] S. Raman, C.H. Malarkey, W.T. Milber, C.W. Nestor, Jr. and P.H. Stelson, At. Data and Nucl. Data Tables **36**, 1 (1987).
[29] G.A. Lalazissis, S. Raman and P. Ring, Atomic Data and Nuclear Data Tables **71**, 1 (1999).
[30] P. Moeller, J.R. Nix, W.D. Myers and W.J. Swiatecki, Atomic Data and Nuclear Data Tables **59**, 185 (1995).
[31] O. Moreno, P. Sarriguren, R. Alvarez-Rodriguez and E. Moya de Guerra, Phys. Rev. C, **73**, 054302 (2006).

TABLE I. Double beta processes involving Xe isotopes, with their experimental half-lives [5,6] and Q-values from experimental masses [7]. When a β^+/β^+ transition is indicated, β^+/EC and EC/EC are also allowed (with Q-values 1.022 MeV and 2.044 MeV lower than the one shown, respectively).

Transition	2β-process	$T_{1/2}$ (yr) exp.	Q-value [MeV]
$^{\mathbf{124}}\mathbf{Xe} \rightarrow {}^{124}$Te	β^+/β^+	$> 2.0 \times 10^{14}$ [5]	2.866
$^{\mathbf{126}}\mathbf{Xe} \rightarrow {}^{126}$Te	EC/EC	—	0.897
^{128}Te $\rightarrow {}^{\mathbf{128}}\mathbf{Xe}$	β^-/β^-	$= 2.5 \pm 0.3 \times 10^{24}$ [6]	0.867
^{130}Te $\rightarrow {}^{\mathbf{130}}\mathbf{Xe}$	β^-/β^-	$= 0.9 \pm 0.1 \times 10^{21}$ [6]	2.529
^{130}Ba $\rightarrow {}^{\mathbf{130}}\mathbf{Xe}$	β^+/β^+	$> 4.0 \times 10^{21}$ [5]	2.610
^{132}Ba $\rightarrow {}^{\mathbf{132}}\mathbf{Xe}$	EC/EC	$> 3.0 \times 10^{20}$ [5]	0.840
$^{\mathbf{134}}\mathbf{Xe} \rightarrow {}^{134}$Ba	β^-/β^-	$> 1.1 \times 10^{16}$ [5]	0.830
$^{\mathbf{136}}\mathbf{Xe} \rightarrow {}^{136}$Ba	β^-/β^-	8.1×10^{20} [5]	2.468

TABLE II. Quadrupole deformation β of the $^{124-142}$Xe equilibrium shapes from a HF(Sk3)+BCS calculation obtained with fixed pairing gaps Δ as well as with fixed pairing strengths G. Results from Refs. [29] and [30] are also given for comparison. Also given are the experimental values obtained from B(E2) transitions [28].

A	$\beta_{th.}$ (Δ fixed)		$\beta_{th.}$ (G fixed)		$\beta_{th.}$ [29]	$\beta_{th.}$ [30]	$\lvert\beta_{exp.}\rvert$
	prolate	oblate	prolate	oblate			from B(E, $2_1^+ \rightarrow 0_1^+$) [28]
124	0.24	-0.19	0.22	-0.17	0.215	0.208	0.264 (8)
126	0.19	-0.18	0.18	-0.15	0.186	0.170	0.1881 (30)
128	0.16	-0.16	0.15	-0.12	0.160	0.143	0.1837 (49)
130	0.13	-0.13	0.11	-0.10	0.128	-0.113	0.169 (6)
132	0.11	-0.10	0.07	-0.10	-0.070	0.000	0.1409 (46)
134	0.05	-0.05	0.01	-	0.000	0.000	0.120 (10)
136	0.00	-	0.00	-	-0.001	0.000	0.086 (19)
138	0.03	-	0.01	-	-0.002	0.000	0.0309 (18)
140	0.15	-0.10	0.12	-	0.104	0.116	0.1136 (25)
142	0.17	-0.12	0.16	-	0.141	0.145	-

TABLE III. Pairing parameters for the HF+BCS calculation in $^{124-142}$Xe. Pairing gaps $\Delta_{\nu,\pi}$ are obtained from experimental binding energies [7]. The pairing strengths $G_{\nu,\pi}$ are those reproducing these gaps at the ground state deformation, which is also indicated (see text for details).

A	Δ_ν [MeV]	Δ_π [MeV]	$\beta_{th.}$ gs	G_ν [MeV]	G_π [MeV]
124	1.32	1.35	0.24	0.114	0.132
126	1.31	1.33	0.19	0.111	0.133
128	1.27	1.32	0.16	0.108	0.130
130	1.25	1.31	0.13	0.108	0.129
132	1.18	1.24	0.11	0.107	0.125
134	1.01	1.12	0.05	0.107	0.119
136	1.44	0.98	0.00	0.121	0.112
138	1.00	1.20	0.03	0.098	0.120
140	0.96	1.06	0.15	0.086	0.144
142	1.03	1.06	0.17	0.084	0.116

TABLE IV. Calculated summed GT^- and GT^+ strengths (in $g_A^2/(4\pi)$ units) for the ground state and the first 0^+ excited state (in brackets) of $^{124-142}$Xe, from a HF(Sk3)+BCS(G) calculation. The difference between both summed strengths is compared with the value of $3(N-Z)$ to check the fulfillment of the Ikeda sum rule (in percentage).

A	ΣGT^-	ΣGT^+	$\Sigma GT^- - \Sigma GT^+$	$3(N-Z)$	%
124	48.62	1.15	47.47	48	98.90
	(48.34)	(0.84)	(47.50)		(98.96)
126	54.33	0.78	53.55	54	99.17
	(54.23)	(0.71)	(53.52)		(99.11)
128	60.16	0.60	59.56	60	99.26
	(60.18)	(0.61)	(59.57)		(99.27)
130	66.12	0.54	65.58	66	99.36
	(66.15)	(0.56)	(65.59)		(99.38)
132	72.12	0.51	71.61	72	99.46
	(71.83)	(0.46)	(71.37)		(99.13)
134	78.14	0.48	77.65	78	99.56
136	83.59	0.47	83.12	84	98.95
138	88.92	0.44	88.48	90	98.31
140	94.69	0.65	94.04	96	97.96
142	100.46	0.43	100.03	102	98.07

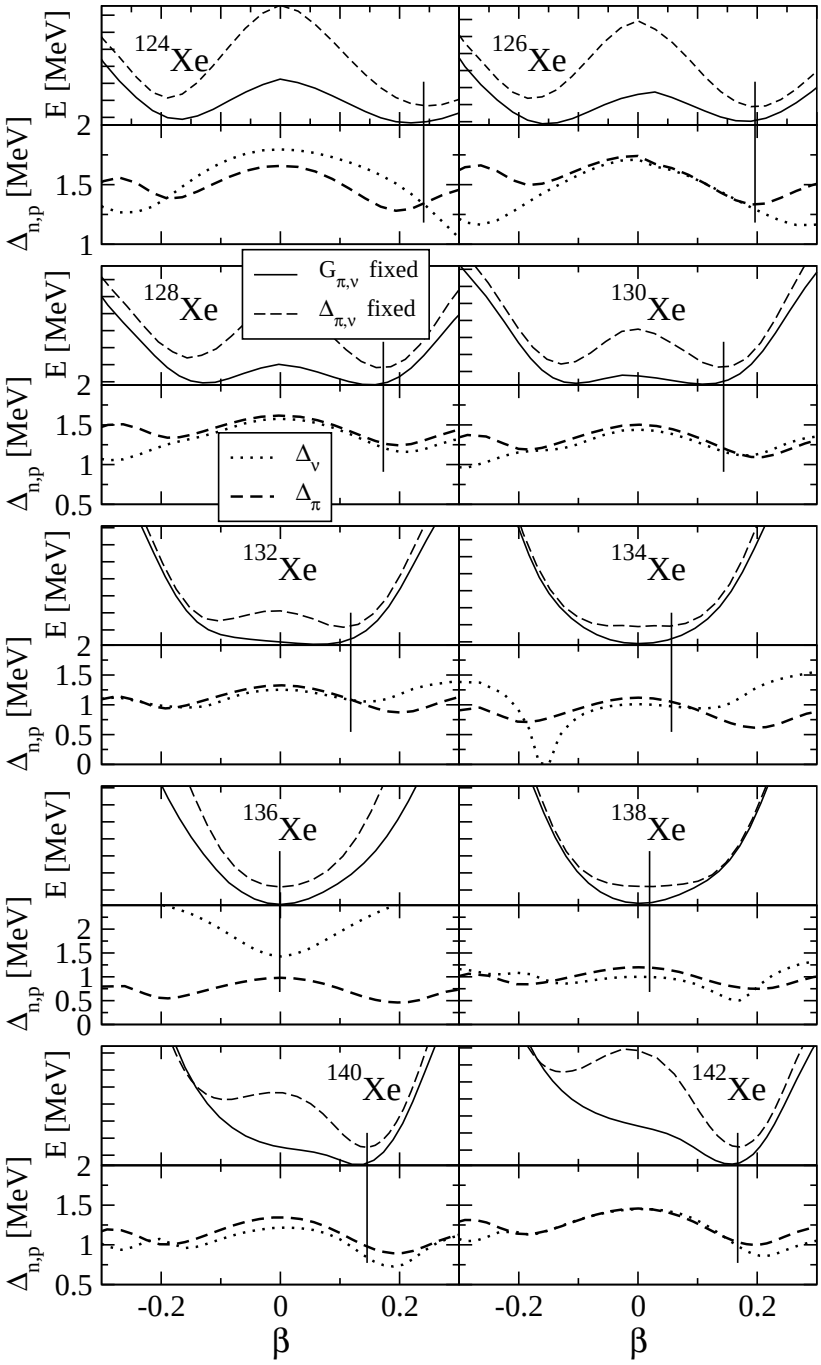

FIG. 1. HF(Sk3)+BCS energy of the isotopes $^{124-142}$Xe as a function of the quadrupole deformation β for fixed pairing gap (dashed line) and for fixed pairing strength (solid line) treatments (with 1 MeV of separation between absolute minima), as well as deformation dependence of pairing gaps from the fixed strength calculation (dashed line for proton gap, dotted line for neutron gap). The scale in the vertical axis is 1 MeV between two ticks. Vertical lines indicate ground states from the fixed gap calculation.

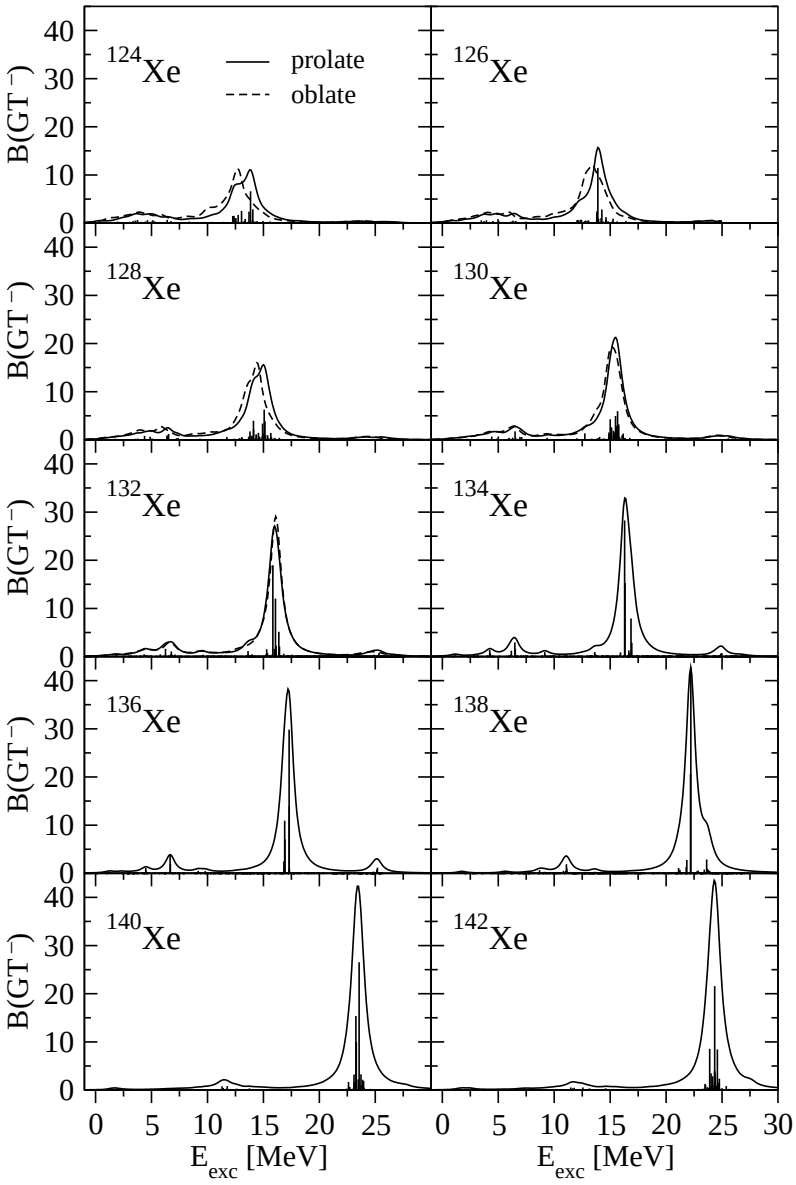

FIG. 2. Discrete and gaussian-folded Gamow-Teller strength distributions B(GT$^-$) for $^{124-142}$Xe, from a HF(Sk3)+BCS(G) calculation. Two equilibrium deformations appear for $^{124-132}$Xe, the solid line and the discrete spectrum corresponding to the prolate shape, and the dashed line corresponding to the oblate shape. The calculations for ^{134,136,138}Xe correspond to spherical shapes, while those for ^{140,142}Xe correspond to prolate shapes (see Table II).

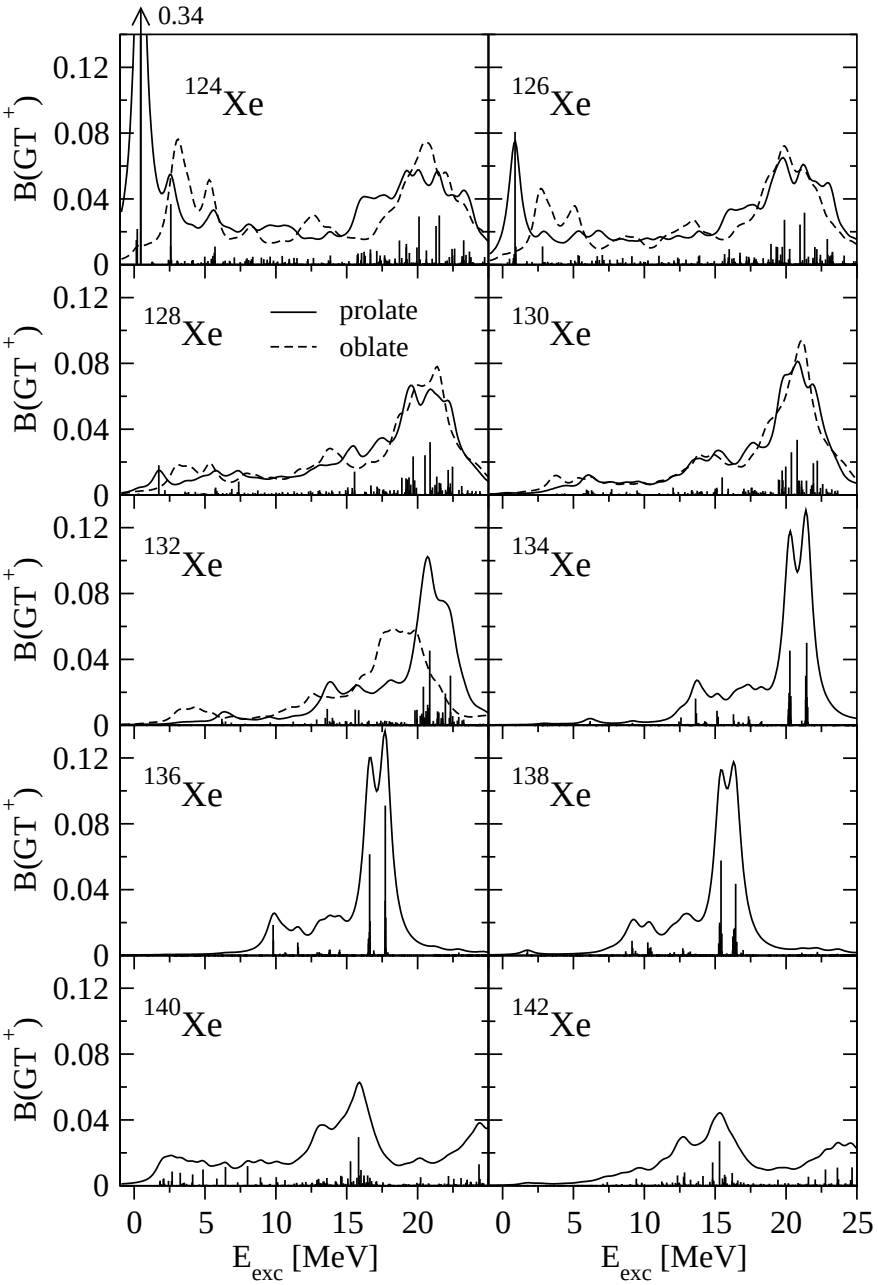

FIG. 3. The same as in fig. 2 but for GT^+ strength distributions.

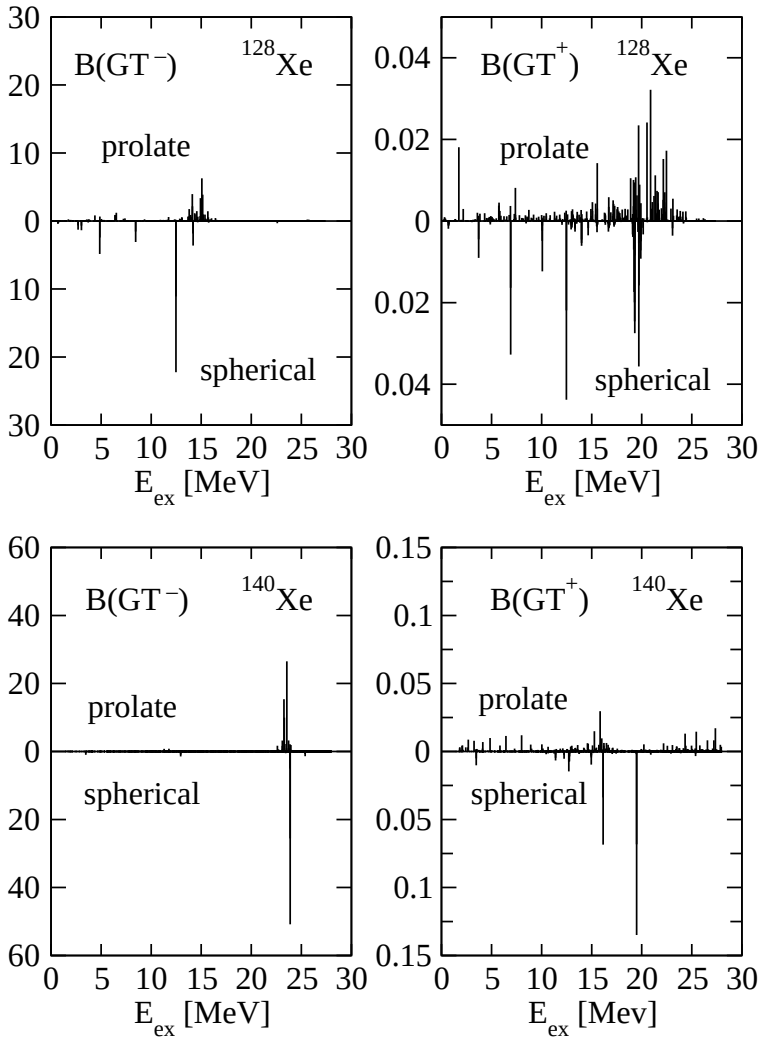

FIG. 4. GT strength distributions in ^{128}Xe (upper panels) and ^{140}Xe (lower panels). Left panels show GT$^-$ strengths, while right panels show GT$^+$ strengths. Calculations with prolate (spherical) shapes are plotted upward (downward), respectively.

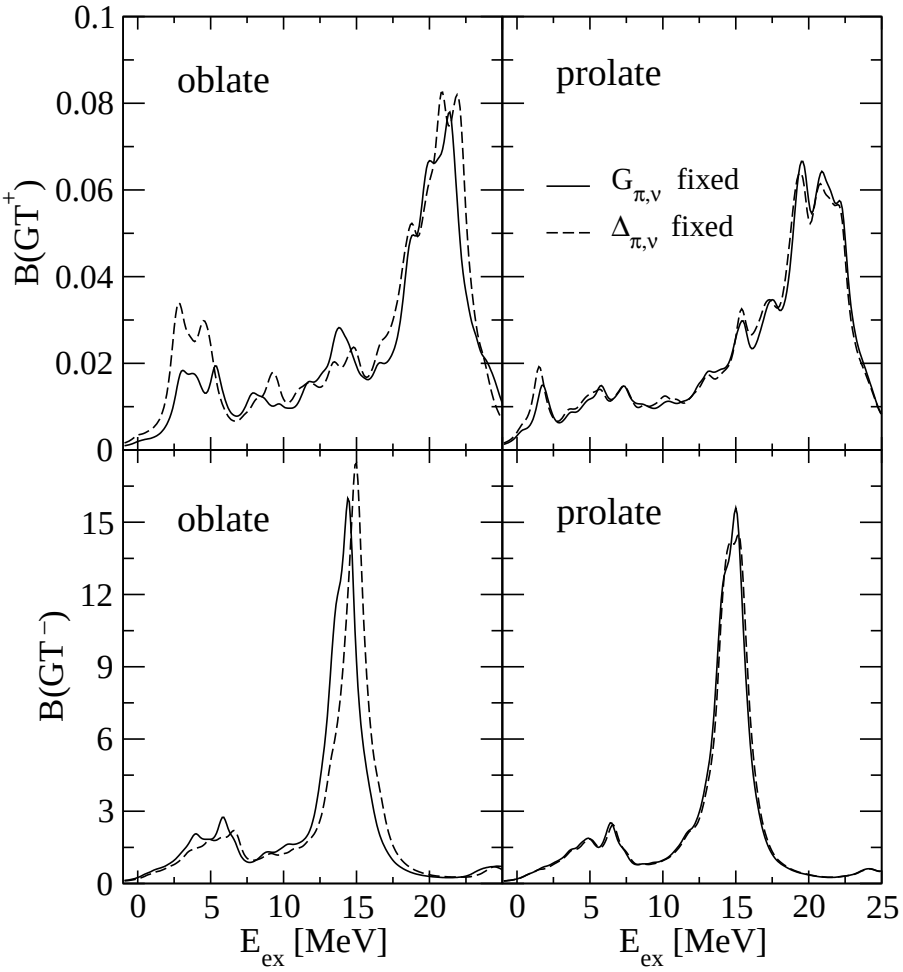

FIG. 5. Gaussian-folded Gamow-Teller strength distributions $B(GT^{\pm})$ in $g_A^2/(4\pi)$ units for both equilibrium shapes of ^{128}Xe, from a HF(Sk3)+BCS(G) calculation (solid line) and a HF(Sk3)+BCS(Δ) calculation (dashed line).